Journal of Thermal Analysis and Calorimetry (2024) 149:9297–9306
https://doi.org/10.1007/s10973-024-13541-6

Ecofriendly composites based on poly (lactic acid) with nano-zirconium phosphate and nano-zinc oxide/zirconium phosphate: physicochemical and aging characteristics

L. C. Mendes[1] · D. M. Mariano[1] · D. F. S. Freitas[1] · G. A. V. Albitres[1] · M. I. B. Tavares[1] · E. E. Garcia[1]

Received: 19 October 2023 / Accepted: 27 July 2024 / Published online: 19 August 2024

Abstract
The search for sustainable polymers to replace those of fossil origin has been constant. Poli (lactic acid) (PLA) is one of the alternatives since it is a biodegradable and ecofriendly polymer. This work intended to aggregate zinc oxide (ZnO) and zirconium phosphate (ZrP) as a tentative to improve PLA crystallization and ultraviolet light stability. To easy the incorporation of ZnO in the ZrP the last one was pre-expanded with *Jeffamine* and following melting extruded PLA composites were prepared. X-ray fluorescence spectroscopy (EDX) showed that incorporation of ZnO (around 50%) in the host filler was successful. Carbonyl absorbance ratio revealed some PLA degraded during the processing. This ratio also increased by exposure to ultraviolet lamps, but ZnO showed best stabilization in the PLA/E-A/ZrP/ZnO. X-rays diffraction revealed that fillers pre-expanded with *Jeffamine* promoted better dispersion but some reduction on the PLA thermal stability was noticed. Fillers promoted a slight increment of the PLA glass transition temperature. The precursor PLA presented a unique melting peak and low degree of crystallinity (around 4%). Either by compression or by extrusion, PLA lonely and in the composites presented two melting peaks identified as α' and α crystalline arrangements and an increase of crystallinity degree was achieved. The material addresses potential application as sustainable alternative for packaging industry.

Keywords PLA · Zirconium phosphate · Nano zinc Oxide · Ether-amine

Introduction

Society, researchers, and industry are increasingly focused in finding solutions to reduce the effects of the use and disposal of conventional plastic waste. The substitution of traditional plastics for bio-based and/or biodegradable materials is one the proposal [1]. Poly (lactic acid) (PLA) has been used as alternative as ecofriendly thermoplastic. Lactic acid—obtained from bacterial fermentation of carbohydrates such as glucose, sucrose or galactose—is a source for the PLA synthesis [2, 3].

PLA was embedded with titanium dioxide (TiO2) and zinc oxide (ZnO) to recovering polluted water. Around 1.5% of this material was able to adsorb 98% of methylene blue [4]. Medeiros et al. developed electrospinning fiber based on blend of copoly (butylene adipate/butylene terephthalate) (PBAT)/PLA filled with rutile titanium dioxide and magnetite iron oxide addressed to photocatalytic degradation of environmental contaminants [5].

Bio based elastomeric blend of PLA with ferulic acid derivatives (FDA) was studied by Gallos and co-authors. Treated and no treated hemp fibers with FDA was added to the that blend, but no have significant action on the fibers dispersion and the mechanical properties were achieved [6]. Bagasse cellulose was modified with bifunctional glycidyl methacrylate and used as bio-reinforcing agent in PLA composites. Tensile strength increased, while modulus decreased according to the filler content [7].

As reinforcing agent, graphene (GR) and ferrite modified with magnesium/zinc (MZF) were incorporated into PLA matrix. The composites exhibited excellent microwave absorption and mechanical properties [8]. To improve flammability and brittleness, Xu et al. developed composites based on PLA containing modified kapok fibers and as prepared phosphonamide flame retardants. Flame retardant

✉ L. C. Mendes
lcmendes@ima.ufrj.br

[1] Instituto de Macromoléculas Professora Eloisa Mano, Centro de Tecnologia, Universidade Federal Do Rio de Janeiro, Bloco J, Ilha Do Fundão, Rio de Janeiro, RJ 21941-598, Brazil

presented gas-phase flame retardancy and condensed-phase barrier effect during the combustion process [9].

TBT (tetra butyl titanate) or TDI (2,4-toluene diisocyanate) were experienced as compatibilizer in poly(lactic acid) (PLA)-poly (propylene carbonate) (PPC) block copolymer. Mechanical properties, crystallinity and interface were dependent on the TBT and TDI content [10]. Oligo (trimethylene sebacate) was synthesized and applying as plasticizer for PLA. Although, the increase of elongation at break and crystallinity degree were attained a slight decrease of thermal stability and storage modulus were seen [11].

Mysiukiewicz et al. studied the effect of the oil extracted from linseed waste on PLA crystallization. The addition at least 17.7 mass% notably increased its crystallinity and promoting the growth of crystallites [12]. ZnO nanoparticles has been gaining importance in the scientific and industrial sectors. Kavitha et al. published a review on plant-mediated zinc oxide nanoparticles and their antibacterial potency. The author highlighted a series of applications in the solar, optical, electrical, and chemical sectors [13].

In other review, Smaoui et al. reported the action of ZnO as bio-safe material against photocatalysis and photooxidation [14]. Shanshool et al. described that ZnO gathers electrical and optical properties besides to be a powerful ultraviolet absorber at 368 nm. These features lead it as a promising material for application in ultraviolet laser diode and light-emitting diodes [15].

Through phytofabrication, Abdelghany and co-authors studied the ZnO nanoparticles activity as antioxidant, anticancer and antimicrobial against pathogenic microorganism. The authors registered good antibacterial activity against various gram positive and negative bacteria [16]. A review describing the action of ZnO nanoparticles as shield against ultraviolet radiation in cotton textile was published by Nasirzadeh and co-authors. It was signalized that the level of protection depends on the yarn structure, woven fabric and porosity, textile impurity and washing conditions besides the ZnO physicochemical features [17].

Khan et al. prepared nanorods of ZnO by microwave techniques at a range of power (300 W, 360 W, 450 W, and 540 W). They observed that the maximum ultraviolet protection in cotton fabric coated with ZnO (540 W) with reduction of UV transmittance around seven times [18]. Two-dimensional zirconium and titanium phosphate has attracted great attention. As a lamellar solid, their structural arrangement furthers the entrance of many guest molecules yielding new chemical functionality [19–21].

Liu et al. synthesized zirconium phosphate in presence of lanthanum nitrate to produce lanthanum-modifying zirconium phosphate. The author monitored the Zr:La molar ratio for water defluorination. From adsorption–desorption cycles, the better adsorption efficiency (above 80%) was found for the phosphate LamZrP2-1 [22]. Liu and co-authors studied composites of zirconium phosphate (ZrP) and zirconium phenyl phosphonate (ZrPP) with nickel/tungsten (Ni–W) for electrodeposition coatings in steel sheets. The authors reported that Ni–W/ZrPP coating showed the better corrosion and wear resistance [23]. Lee et al. developed inorganic composites at different proportions based on ZrP and tubular halloysite clay (THC) searching to improve fire resistance. The coating prepared with hallosysite:zirconium, 1:1 ratio, presented the best performance as intumescent fire-retardant [24].

The aim of this investigation was to introduce improvement on the PLA crystallization and light stability through the incorporation of zinc oxide (ZnO) and zirconium phosphate (ZrP) by preparing melting extruded composites. Physicochemical characteristics and ultraviolet light stabilization were evaluated. The material could be considered as alternative sustainable for packaging industry.

Experimental

Materials

Poly(lactic acid) (PLA), Oeko Bioplásticos, Phosphoric acid (H_3PO_4), zirconium (IV) oxide chloride 8-hydrate ($ZrOCl_2{\cdot}8H_2O$), ethyl alcohol, nano zinc oxide (ZnO, < 100 nm) and ether-amine (Jeffamine M-600, 600 g mol^{-1}) (Sigma-Aldrich Co.) were used.

Methods

Synthesis and modification of layered zirconium phosphate

The lamellar-zirconium phosphate was synthetized by reaction between phosphoric acid solution 12 M and zirconium oxychloride, at ratio Zr/P = 18, kept under reflux at 110 °C, under stirring, for 24 h [25]. It was previously modified with *Jeffamine* with subsequent addition of nano-ZnO [26, 27].

Nanocomposite and specimen preparation

For better filler dispersion and distribution, a masterbatch with settled amount of filler was processed in Haake internal mixing—Haake Polylab QC, using roller, 60 rpm, 170 °C, 7 min to get 2 mass% of filler in the final composite. Melt extruded PLA composites were processed with processing window at 160–170 °C, 60 rpm, labeled as PLA, PLA/ZrP, PLA/E-A/ZrP and PLA/E-A/ZrP/ZnO. The sample was dried, at 80 °C, for 24 h and compression specimen following ASTM D638-10 (type V) was prepared in Carver press, at 190 °C, with time processing of ten minutes including heating and cooling cycles.

Characterization

X-ray fluorescence spectroscopy (EDX) The chemical composition of the samples was measured using fluorescence Instruments, model EDX-720 (Shimadzu). The analysis was carried out in powder form, free of water and under vacuum for 320 s.

Infrared spectroscopy (FTIR) Infrared spectroscopy was performed in Perkin Elmer equipment, model Frontier. The spectrum was taken by KBr disk, in the range of 4000–400 cm^{-1} with 50 scans and 4 cm^{-1} of resolution. The absorbance ratio between absorptions at 1748 cm^{-1} (C = O band) and at 2996 cm^{-1} (C–H band) was performed searching if some PLA degradation occurred.

Wide-angle X-ray diffraction (WAXD) X-rays diffraction pattern was obtained using Rigaku equipment, model Ultima IV, CuKα radiation with wavelength (1.5418 Å) Ni filter, 30 kV voltage and current of 15 mA, 2θ between 2 and 50° and resolution of 0,05º. Bragg equation $n = 2d_{hkl}$ sen θ (n—diffraction order; d_{hkl}—interlayer spacing; θ—Bragg angle) was used to determine interlayer spacing ($d_{spacing}$). Through Debye–Scherrer equation $\tau = K * \lambda / \beta * \cos\theta$ (K = constant, 0.9; λ = mean value of the wavelength of Cu radiation in the apparatus, 1.5418 Å, β = full width at half maximum of peak (in radians) and θ = Bragg angle) the crystal was evaluated.

Thermogravimetric (TG/DTG) TA instrument, model Q500 was used for evaluating the sample thermal stability, from 10 to 700 °C, at 10 °C min^{-1}, with nitrogen as carrying gas. Degradation temperatures at 10, 25 and 50 of mass loss and T_{max} were registered.

Differential scanning calorimetry (DSC) TA Instruments, model Q1000 was applied to monitor calorimetric parameters. Three thermal cycles were performed. Firstly, the sample was heated from 10 to 190 °C, 10 °C min^{-1}, under nitrogen atmosphere, maintained at that temperature for 2 min, to eliminate the thermal history. A cooling cycle was carried out until 0 °C, at 10 °C min^{-1}. A last heating cycle was conducted in the same conditions of the initial one. Glass transition, crystallization and melting temperatures (T_g, T_c and T_m) were registered. Normalized crystallinity degree (X_c) was calculated considering the ratio between the experimental enthalpy of fusion and the enthalpy of fusion of 100% crystalline PLA (93.6 $J{\cdot}g^{-1}$) [28].

Ultraviolet light stabilization Aging was performed in ultraviolet dark chamber, model SP-204, coupled with ultraviolet lamps of 365 nm. Both sides of the specimen were exposed to UV radiation, for 120 h. After that, the specimen was dissolved in chloroform. The solution was taken for analysis in equipment described above. The absorbance ratio between absorptions at 1748 cm^{-1} (C = O band) and at 2996 cm^{-1} (C–H band) was determined to monitor the effect of UV radiation. The average and standard deviation of three measurements was considered.

Results and discussion

X-ray fluorescence spectroscopy (EDX)

Table 1 shows the fillers' elemental composition in the composites and the Zr/P ratio. ZrP galleries was significantly modified by Jeffamine since that Zr/P ratio was reduced to one third. Also, ZnO was incorporated to E-A-ZrP, but the reduction of Zr/P ratio was a little bit lower. Around 50 mass% of ZnO was incorporated indicating that ZrP modification was successful.

Infrared spectroscopy (FTIR)

Figure 1a–c shows FTIR spectra of fillers and composites. PLA spectrum shows absorptions at 3504 cm^{-1} (O–H stretching), 2996 and 2951 cm^{-1} (C–H asymmetric and symmetric stretching), 1748 cm^{-1} (C = O stretching), 1412 cm^{-1} (C–H bending), 1379 cm^{-1} (C–H bending), 1357 cm^{-1} (C–H bending), 1263, 1180, 1081 and 1043 cm^{-1} (C–O stretching and O-C = O stretching), 865 and 753 cm^{-1}, C–C bending of amorphous and crystalline portion, respectively [29–34]. ZrP presented a series of absorptions at 3595, 3511 and 1617 cm^{-1} (asymmetric/symmetric bending of water in the interlayer region), 3153 cm^{-1} (stretching of the hydrogen bonding between H–O–H and P–OH group), 1250 cm^{-1} (P–O–H bending), 1112, 1074 and 1050 cm^{-1} (PO42- asymmetric stretching) and 980 and 968 cm^{-1} (PO4 symmetric stretching). Jeffamine-modifying ZrP showed absorptions at 4000–3000 cm^{-1}, 3000–2500 cm^{-1}, 1500–1300 cm^{-1}, 1250 cm^{-1}, 1200–900 cm^{-1}, P–O (phosphate) and C–O–C (Jeffamine), 600–700 cm^{-1}. ZnO displayed little and low intense absorptions at 3436 cm^{-1}, 496 cm^{-1} and 437 cm^{-1} [20, 35, and 36].

The close observation of the PLA/ZrP, PLA/E-A/ZrP and PLA/E-A/ZrP/ZnO) infrared spectra (see side windows)

Table 1 X-ray fluorescence of fillers' elemental percentage

Sample	Zr	P	Zn	Zr/P ratio
Element mass/%				
PLA/ZrP	56	32	–	1.75
PLA/E-A/ZrP	31	50	–	0.62
PLA/E-A/ZrP/ZnO	13	26	46	0.50

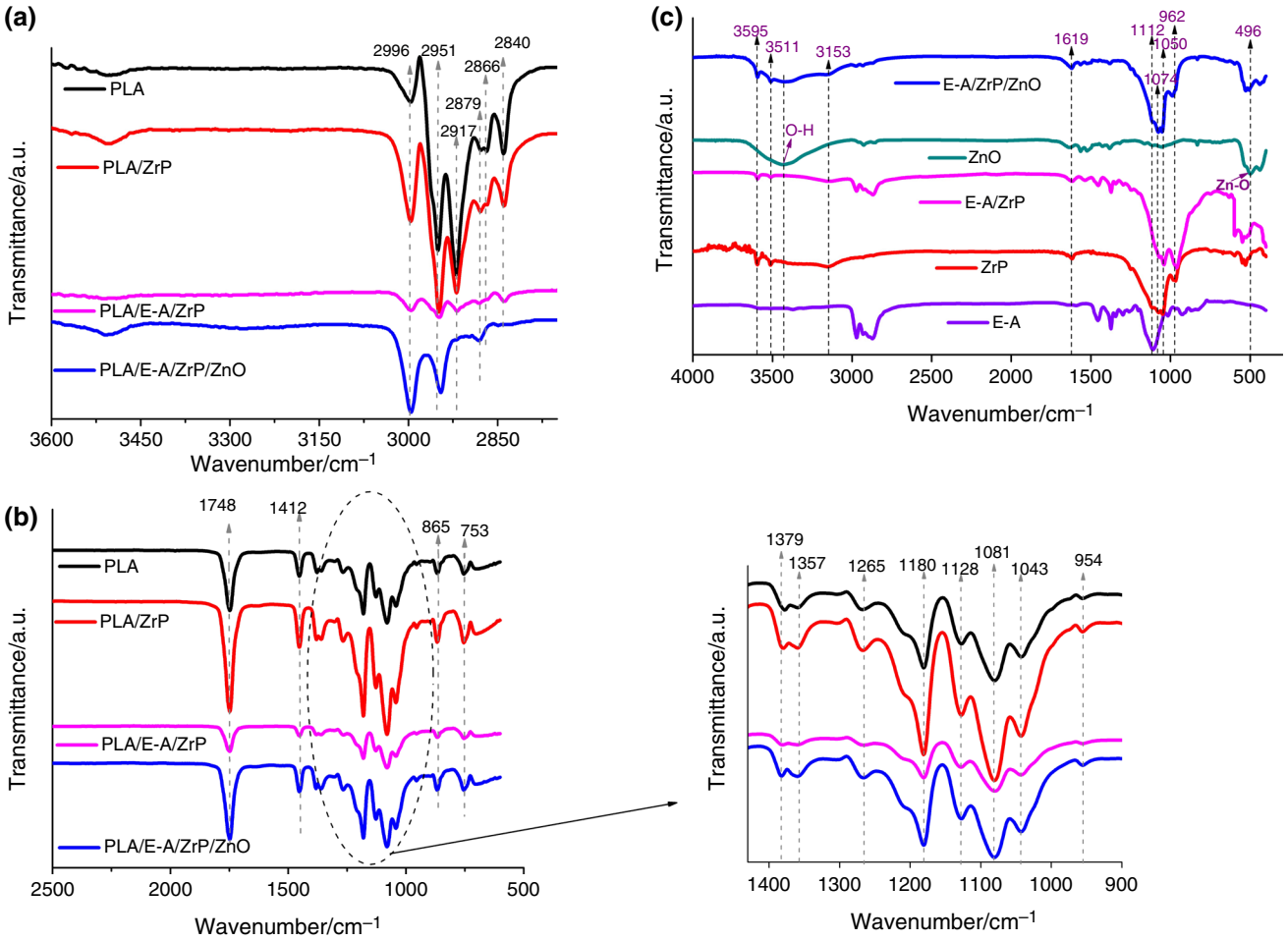

Fig. 1 Fillers, PLA and composites infrared spectra

revealed that fillers' absorptions are superimposed by the PLA ones probably owing to their low content. Ahmadzadeh et al. investigated the role of the different amount of ZnO nanoparticles (0, 2, 4 and 6 mass%) on degradation of poly(lactic acid)/polycaprolactone (PLA/PCL, 80/20 mass/mass%) blend. The authors registered no motion but progressive intensification of carbonyl absorptions with ZnO content attributing it as degradative action of nanoparticles through the formation of lactide molecules, oligomeric ring and acetaldehyde groups. It was concluded that concentration, melt mixing route, dispersion and distribution of ZnO nanoparticles had a great influence on the blend mechanical, rheological and degradation characteristics [34].

To assess if there was some action of fillers on PLA chains during the composites processing, the absorbance relationship between absorptions at 1748 cm^{-1} (C=O band) and at 2996 cm^{-1} (C–H band) was performed. This sequence was found PLA (2.7 ± 0.4), PLA/ZrP (4.5 ± 2.3), PLA/E-A/ZrP (4.0 ± 1.6) PLA/E-A/ZrP/ZnO (8.5 ± 2.5). Considering the margin of error, we infer that all filler in some extent provoked a catalytic degradation of the PLA chains during the processing, but this action was more emphatic for the E-A/ZrP/ZnO filler.

Wide-angle X-ray diffraction (WAXD)

Recently, we published an article on the incorporation of ZnO in zirconium phosphate [20]. Herein, to better understand, the diffraction patterns of the fillers at 2θ (2–15°) are shown (Fig. 2a). ZnO presented a low intensity 2θ angle around 13°. ZrP basal plane appeared around 12° ($d_{spacing}$ 0.74 nm, crystal size 302 nm). ZrP was pre-expanded with *Jeffamine* (E-A/ZrP). With lesser intensity and slightly displaced (11.65°), ZrP basal peak was detected but a series of new 2θ angles emerged around 6.32, 4.70 and 3.15°. After its modification with ZnO, the filler E-A/ZrP/ZnO only exhibited low intensity 2θ angles of Zr (11.75°) and ZnO (13°).

Diffraction patterns of PLA and composites are shown in Fig. 2b. PLA presented amorphous halo indicative of

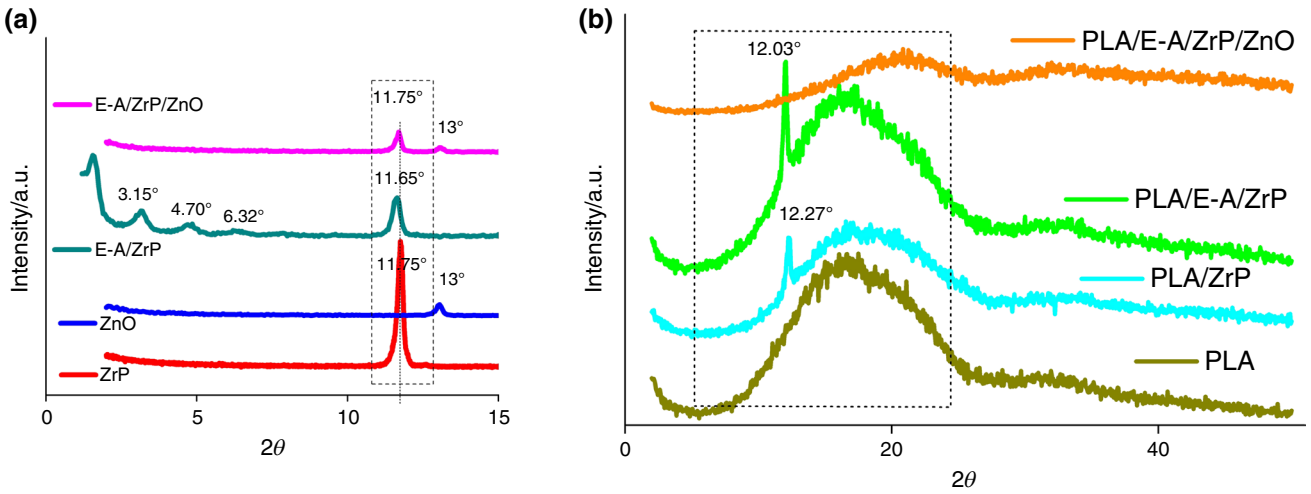

Fig. 2 WAXD of fillers (**a**) and PLA, PLA composites (**b**)

predominant amorphous matter or crystalline matter with imperfect and extremely small crystals as reported elsewhere [37, 38]. The same was observed for the composites PLA/ZrP and PLA/E-A/ZrP but in both ZrP basal plane was seen. For composite PLA/E-A/ZrP/ZnO, the amorphous halo of PLA appeared but no filler diffraction angles were detected. Considering the filler dispersion into PLA matrix, the best systems were PLA/E-A/ZrP and PLA/E-A/ZrP/ZnO. For PLA/E-A/ZrP composite, the disappearance of 2θ angles at 6.32, 4.70 and 3.15° (planes with high $d_{spacing}$) was fomented by the entrance of PLA chains into the preexpanded portion of the phosphate, but some original ZrP remained. For PLA/E-A/ZrP/ZnO, since the anchoring of ZnO to E-A/ZrP disturbed its arrangement—low intense peak was understood as lower packing degree—, the addition of PLA promoted the vanish of the ZrP and ZnO diffraction angles which was seen as improvement of filler dispersion.

Thermogravimetric (TGA)

Figure 3a and b exhibit the mass loss and derivative curves. The mass loss curves of PLA and PLA/ZrP are superimpose along the temperature axis with higher thermal stability. PLA/E-A/ZrP and PLA/E-A/ZrP/ZnO curves are detached from others being the last one with lower thermal stability. It is important to emphasize that thermal degradation occurred in two steps (see side frame). The lowest decay was associated to the release of absorbed water, while the highest one to the polymer/filler. The derivative curves showed a progressive gradation in the maximum peak temperature (T_{max}): PLA > PLA/ZrP > PLA/E-A/ZrP > PLA/E-A/ZrP/ZnO. Table 2 displays the temperature at 10, 25 and 50 mass% of mass loss. At all range, PLA and PLA/ZrP presented similarity of mass loss. PLA/E-A/ZrP and PLA/E-A/ZrP/ZnO composites revealed lower stability than those ones but the sample with E-A/ZrP/ ZnO having the lowest degradation temperature.

Liu et al. prepared composites based on PLA embedded with cellulose nanofibrils (CNF), and lignin–cellulose nanofibrils (LCNF). The authors revealed that the thermal stability of PLA/LCNF composite was higher than PLA, while lower values was found for PLA/CNF one [39]. Gonzalez et al. studied composites based on PLA with nano titanium oxide (< 100 nm) (PLA/TiO_2). Two steps of degradation were registered and T_{max} showed a slight increase [40]. Tarani et al. investigated the action of nano zinc and titanium oxide (ZnO, < 100 nm, and TiO_2≈3–5 nm) and silver nanoparticles (Ag, ≈ 10 nm) in PLA composites. TiO_2 and Ag nanoparticles did not affect the PLA degradation, but ZnO showed a catalytic action decreasing the polymer thermal stability [41].

Herein, the composites containing E-A/ZrP and E-A/ZrP/ZnO fillers were those with lower thermal stability. We understood that both the presence of *Jeffamine*—long chain amine used as pre expander of ZrP–and the catalytic degradation of filler contributed to the reduction of thermal stability. *Jeffamine* could have promoted PLA chains disentanglement favoring the catalytic degradation of ZnO on PLA chains.

Differential scanning calorimetry (DSC)

To better understand the DSC data, it was included the calorimetric curves of pristine PLA, pristine PLA (compression film), PLA and PLA composites (extruded samples). Figure 4 showed the calorimetric curves of the second heating cycle. Glass transition temperature (Tg) for PLA

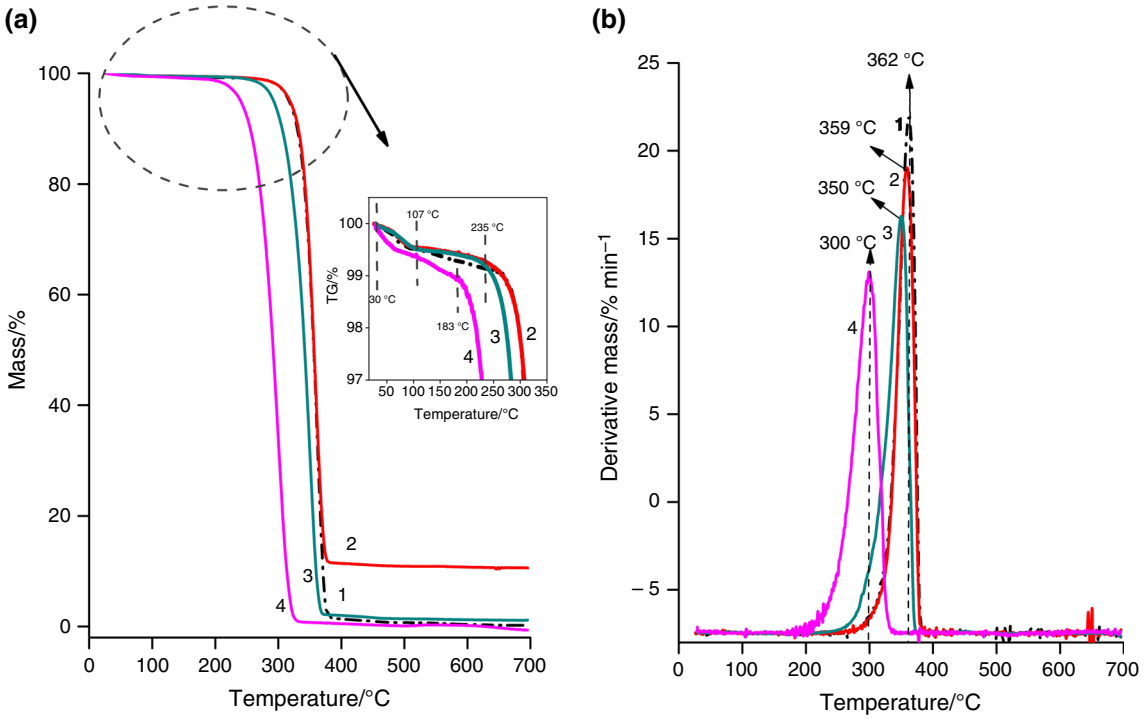

Fig. 3 Mass loss and derivative curves of PLA and PLA composites

Table 2 Thermogravimetric data of PLA and PLA composites

Sample	T10/°C	T25/°C	T50/°C	Tmax/°C
PLA	330	345	356	362
PLA/ZrP	332	345	357	359
PLA/E-A/ZrP	306	326	342	350
PLA/E-A/ZrP/ZnO	225	275	292	300

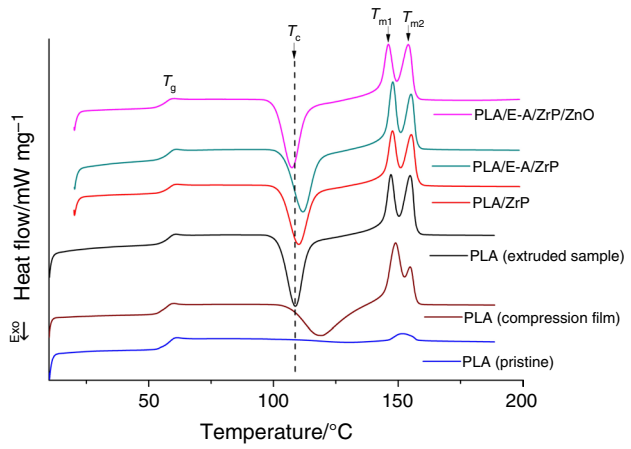

Fig. 4 Calorimetric curves of PLA and PLA composites

(pristine), PLA (compression film) and PLA (extruded sample) occurred in the same range.

Crystallization temperature (Tc) was absent in the pristine PLA. PLA compression film presented enlarged crystallization peak. Extruded PLA and composites exhibited a sharp crystallization peak. The Tc of composites were dependent on the kind of filler. Melting of pristine PLA presented a broad and low intensity peak. PLA compression film revealed a twin melting peak with different intensity. Similarly, extruded PLA and composites disclosed a twin melting peak with resembling intensity.

Table 3 displays the calorimetric data. Unprocessed, compression and extruded PLA revealed the same Tg value. Tg of PLA composites emerged 7–9 °C higher than PLA. Tc was absent in pristine PLA. For compression PLA, Tc appeared at higher temperature if compared to those showed by extruded PLA and PLA composites. For extruded samples, PLA and PLA/ZrP had similar Tc but PLA/E-A/ZrP and PLA/E-A/ZrP/ZnO presented the highest and the lowest Tc, respectively. Enlarged and low intense melting peak was registered for pristine PLA. Two melting temperatures were noticed by compression and extruded samples without significant difference for each melting peak. Degree of crystallinity (Xc) was extremely low for pristine PLA. Compression PLA film presented Xc around 34% but the lowest melting peak showed Xc more than four times larger if compared to the second one.

Table 3 DSC data of PLA and PLA composites

Sample	T_g/°C	T_c/°C	T_{m1}/°C	T_{m2}/°C	X_c/%		
					Total	1	2
PLA (pristine)	57	–	–	152	4.4	–	–
PLA (compression)	56	119	149	155	34	28	6
PLA (extruded)	55	109	147	155	38	18	20
PLA/ZrP	64	110	148	155	34	17	17
PLA/E-A/ZrP	64	112	148	155	37	20	17
PLA/E-A/ZrP/ZnO	62	107	146	154	36	17	19

Extruded PLA and PLA composites exhibited almost constant Xc, in total and for each melting peak.

Solution films of PLA composites with hydroxyapatite (0–4 mass%) were studied by Pandele and co-authors. Calorimetric data revealed a twin melting peak (Tm around 142 and 150 °C) and reduction of crystallinity degree with filler addition [42]. Chu et al. prepared composites based on PLA with nano silver particles (Ag) and nano ZnO. The addition of fillers diminished the glass transition and crystallization temperatures. Although the authors did not comment, the melting peak is composed by a shoulder at lower temperature and a sharp one at higher temperature which decreased when the filler was added [43]. Melting composites of PLA added with doped ZnO with silver and copper (ZnO:Ag/Cu) and plasticizers were studied by Vasile and co-authors. The addition of filler and plasticizers reduced the glass transition and crystallization temperatures. For the composites, two melting peaks appeared, but nothing was commented about the second one. All composites showed increase in Xc associated to the heterogeneous nucleation [44].

Summarizing, the composites showed increase of Tg what was deduced as PLA stiffening. Also, for the composites, although slight variation on Tc was seen this was not decisive on the crystallinity degree. The results highlighted the effect of processing on the melting and crystallization events. Under compression and extrusion, PLA and PLA composites disclosed a twin melting peak and high content of crystalline matter. As published by Meng et al., PLA can crystallize at three different crystalline arrangements α, α' and β. The α crystalline form emerges from melting or solution preparation processes, at temperature upper 120 °C. The helical conformation of α' form is identical to α one, but chain arrangement is lesser. Beta form presented different helical conformation but arises through the stretching of the α form crystal near to the melting temperature [28]. It was supposed that the two melting peaks found in PLA compression, extruded PLA and PLA composites are related to α' form (lower one) and α form (upper one). DSC analysis indicated that the fillers did not have any additional nucleation effect. The increase registered on degree of crystallinity was attributed to the effects of heating and cooling cycles during the processing which contributed to step up the PLA nucleation event.

Ultraviolet light stabilization

Table 4 discloses the ratio between the bands 1748 and 2996 cm^{-1} before and after UV light exposure. The ratios for nonirradiated samples showed the following sequence: PLA/E-A/ZrP/ZnO > PLA/E-A/ZrP and PLA/ZrP > PLA. For irradiated samples, the ratios presented values according to the sequence: PLA > PLA/E-A/ZrP and PLA/E-A/ZrP/ZnO > PLA/ZrP. The relationship between the ratios after and before UV light exposure obeyed this order: PLA > PLA/E-A/ZrP > PLA/ZrP > PLA/E-A/ZrP/ZnO. About UV stabilization efficacy (SE), the calculation was performed as $SE = ratio_{afteraging} - ratio_{beforeaging}/ratio_{beforeaging}$ (×100). All fillers exhibited some stabilization to ultraviolet light if compared to lonely PLA.

Gardette et al. studied melting extrusion composites of PLA with calcium sulphate ($PLA/CaSO_4$, 70/30). Under photooxidation conditions and in the presence of oxygen,

Table 4 Infrared absorbance ratio, relationship between ratios and UV stabilization efficacy

Sample	Infrared absorbance ratio			
	Before aging	After aging	Relationship between aging ratios (after/before)	UV stabilization efficacy/%
PLA	2.7 ± 0.4	11.2 ± 1.8	4.1	− 314
PLA/ZrP	4.5 ± 2.3	5.6 ± 0.8	1.2	− 24
PLA/E-A/ZrP	4.0 ± 1.6	7.9 ± 1.1	2.0	− 98
PLA/E-A/ZrP/ZnO	8.5 ± 2.5	8.0 ± 0.4	0.9	− 6

they were submitted to UV irradiation at wavelength higher than 300 nm. The presence of $CaSO_4$ hastened the PLA degradation process. The surface of the irradiated samples was exposed to ammonia gas leading to the formation of carboxylates and amide groups [30]. Boopasiri et al. developed chloroform casting films of PLA filled with nanocrystalline cellulose (NCC) and modified with ZnO (NCC–ZnO), at 0.25–10 mass%. The NCC–ZnO showed 20–60% of efficiency as UV protection shield for UV-A and UV-B radiations [45].

In summary, the UV light showed deleterious action on PLA chains. Among the composites, PLA/ZrP presented some resistance against UV light. The presence of *Jeffamine* harmed the UV stabilization in the PLA/E-A-ZrP composite probably owing to this action on the PLA chains disentanglement. The better result was found for the composite containing ZnO (PLA/E-A/ZrP/ZnO) which in association with EDX and X-rays diffraction analyses could be related to the amount and dispersion of ZnO.

Conclusions

The aim of this investigation was to introduce new functionality to PLA matrix. Pristine ZrP and its chemical modification with *Jeffamine* and ZnO was carried out following their incorporation into PLA matrix. By calorimetry, PLA crystal arrangement and degree of crystallinity varied which was attributed to the change in the PLA nucleation step. Thermogravimetric and infrared brought insight on the PLA catalytic degradation during PLA processing. The fillers did not show effect on the PLA nucleation. The PLA/E-A/ZrP/ZnO presented the better stabilization against ultraviolet light. The material revealed a potential sustainable application for packaging industry.

Author contributions L.C. Mendes—data discussion and manuscript organization; D.M. Mariano—synthesis and modification of the phosphates/POM analysis; D.F.S. Freitas—nanocomposites' preparation; G.A.V. Albitres—thermogravimetric and calorimetric analyses; M.I.B. Tavares—data discussion and manuscript organization; E.E. Garcia—infrared and aging analyses.

References

1. da Barbosa S, Ferreira E, Luna CB, Siqueira DD, Araújo EM, de França DC, Wellen RM. Annealing effect on PLA/EVA blends performance. J Polym Environ. 2021;30:541–54. https://doi.org/10.1007/s10924-021-02220-4.
2. Brito LM, Tavares MI. Pla-starch microparticles containing clays focusing controlled release of rifampicin. Mater Sci Appl. 2022;13:441–52. https://doi.org/10.4236/msa.2022.137026.
3. Fang T, Liu M, Li Z, Xiong L, Zhang D, Meng K, Qu X, Zhang G, Jin X, Yang C. Hydrothermal conversion of fructose to lactic acid and derivatives: synergies of metal and acid/base catalysts. Chin J Chem Eng. 2023;53:381–401. https://doi.org/10.1016/j.cjche.2021.12.027.
4. Andrade-Guel M, Cabello-Alvarado CJ, Cadenas-Pliego G, Ávila-Orta CA. PLA-ZnO/TiO_2 nanocomposite obtained by ultrasound-assisted melt-extrusion for adsorption of methylene blue. Nanomaterials. 2022;12:4248. https://doi.org/10.3390/nano12234248.
5. Medeiros AR, da Lima F, Rosenberger AG, Dragunski DC, Muniz EC, Radovanovic E, Caetano J. Poly(butylene adipate-co-terephthalate)/poly(lactic acid) polymeric blends electrospun with TiO_2-R/Fe_3O_4 for pollutant photodegradation. Polymers. 2023;15:762. https://doi.org/10.3390/polym15030762.
6. Gallos A, Lannoy O, Bellayer S, Fontaine G, Bourbigot S, Allais F. Fire testing and mechanical properties of neat and elastomeric polylactic acid composites reinforced with raw and enzymatically treated hemp fibers. Green Chem Lett Rev. 2023;16:2164472. https://doi.org/10.1080/17518253.2022.216447.
7. Wang Y, Xu H, Huang L, Han X, Wei Z, Mo Q, Wang X, Li Y. Preparation and properties of graft-modified bagasse cellulose/polylactic acid composites. J Nat Fibers. 2023;20:2164822. https://doi.org/10.1080/15440478.2022.2164822.
8. Ye X, Gao Q, Yang P, Yang C, He E, Ye Y, Wu H. Mechanical and microwave absorbing properties of graphene/MN–zn ferrite/polylactic acid composites formed by fused deposition modeling. J Mater Sci. 2023;58:2525–38. https://doi.org/10.1007/s10853-023-08196-x.
9. Xu K, Yan C, Du C, Xu Y, Li B, Liu L. Preparation and mechanism of toughened and flame-retardant bio-based polylactic acid composites. Polymers. 2023;15:300. https://doi.org/10.3390/polym15020300.
10. Song L, Li Y, Meng X, Wang T, Shi Y, Wang Y, Shi S, Liu L-Z. Crystallization, structure and significantly improved mechanical properties of PLA/PPC blends compatibilized with PLA-PPC copolymers produced by reactions initiated with TBT or TDI. Polymers. 2021;13:3245. https://doi.org/10.3390/polym13193245.
11. Inácio EM, Lima MC, Souza DH, Sirelli L, Dias ML. Crystallization, thermal and mechanical behavior of oligosebacate plasticized poly (lactic acid) films. Polímeros. 2018;28:381–8. https://doi.org/10.1590/0104-1428.04917.
12. Mysiukiewicz O, Barczewski M. Crystallization of polylactide-based green composites filled with oil-rich waste fillers. J Polym Res. 2020;27:374. https://doi.org/10.1007/s10965-020-02337-5.
13. Kavitha A, Doss A, Praveen Pole RP, Pushpa Rani TPK, Prasad R, Satheesh S. A mini review on plant-mediated zinc oxide nanoparticles and their antibacterial potency. Biocatal Agric Biotechnol. 2023;48:102654. https://doi.org/10.1016/j.bcab.2023.102654.
14. Smaoui S, Chérif I, Ben Hlima H, Khan MU, Rebezov M, Thiruvengadam M, Sarkar T, Shariati MA, Lorenzo JM. Zinc oxide nanoparticles in meat packaging: a systematic review of recent literature. Food Packag Shelf Life. 2023;36:101045. https://doi.org/10.1016/j.fpsl.2023.101045.
15. Shanshool HM, Yahaya M, Yunus WM, Abdullah IY. Investigation of energy band gap in polymer/ZnO nanocomposites. J Mater Sci Mater Electron. 2016;27:9804–11. https://doi.org/10.1007/s10854-016-5046-8.
16. Abdelghany TM, Al-Rajhi AM, Yahya R, Bakri MM, Al Abboud MA, Yahya R, Qanash H, Bazaid AS, Salem SS. Phytofabrication of zinc oxide nanoparticles with advanced characterization and its antioxidant, anticancer, and antimicrobial activity against pathogenic microorganisms. Biomass Convers Biorefin. 2022;13:417–30. https://doi.org/10.1007/s13399-022-03412-1.
17. Nasirzadeh N, Monazam Esmaeelpour M, Naseri N, Omari SS. Improving ultraviolet protection properties of cotton textiles using zinc oxide (ZnO) nanomaterials: an approach for controlling occupational and environmental exposures. Int J Environ

Health Res. 2023;34:2067–87. https://doi.org/10.1080/09603123.2023.2211529.
18. Khan MZ, Taghavian H, Fijalkowski M, Militky J, Tomkova B, Venkataraman M, Adach K. Effect of microwave power on bactericidal and UV protection properties of the ZnO nanorods grown cotton fabrics. Colloids Surf A. 2023. https://doi.org/10.1016/j.colsurfa.2023.131135.
19. Amghouz Z, García JR, Adawy A. A review on the synthesis and current and prospective applications of zirconium and titanium phosphates. Eng. 2022;3:161–74. https://doi.org/10.3390/eng301001310.3390/eng3010013.
20. Mariano DM, Freitas DF, Albitres GA, Mendes LC, Tavares MI. Incorporation of nano-zinc oxide in lamellar zirconium phosphate: synthesis and characterization. Mater Sci Appl. 2023;14:346–61. https://doi.org/10.4236/msa.2023.146022.
21. Garcia EE, Albitres GA, Freitas DF, Mariano DM, Mendes LC. Zinc and silver salts-containing lamellar titanium phosphate: a multifunctional filler. Mater Sci Appl. 2022;13:366–88. https://doi.org/10.4236/msa.2022.136021.
22. Liu D, Li Y, Liu C, Li B. Porous lanthanum-zirconium phosphate with superior adsorption capability of fluorine for water treatment. J Colloid Interface Sci. 2023;636:588–601. https://doi.org/10.1016/j.jcis.2023.01.062.
23. Liu B, Yan S, He Y, He T, He Y, Song R, Zhang Z, Li H, Song J, Li Z. Study on wear resistance and corrosion resistance of zirconium phenylphosphonate reinforced Ni–W composite coating. Appl Surf Sci. 2022;603:154483. https://doi.org/10.1016/j.apsusc.2022.154483.
24. Lee YX, Ahmad F, Kabir S, Masset PJ, Onate E, Yeoh GH. Synergistic effects of tubular halloysite clay and zirconium phosphate on thermal behavior of intumescent coating for structural steel. J Market Res. 2022;18:4456–69. https://doi.org/10.1016/j.jmrt.2022.04.097.
25. Mariano DM, Freitas DF, Mendes LC. Nanocomposite of polypropylene/octadecylamine lamellar-zirconium phosphate: influence of nanofiller and screw speed. J Compos Mater. 2017;52:701–11. https://doi.org/10.1177/0021998317713832.
26. Mariano DM, Freitas DF, Mendes LC, Carvalho AL, Ramos FJ. Investigation on structural, morphological and relaxometric properties of lamellar ZrP modified with long chain amine. Mater Res. 2019;22:e20180493. https://doi.org/10.1590/1980-5373-mr-2018-0493.
27. Carvalho AL, Freitas DF, Mariano DM, Mattos GC, Mendes LC. The influence of zinc gluconate as an intercalating agent on the structural, thermal, morphologic, and molecular mobility of lamellar nanofiller. Colloid Polym Sci. 2018;296:1079–86. https://doi.org/10.1007/s00396-018-4319-6.
28. Meng L, Zou F, Chen M, Li Y, Wang Y, Sun X, Wang X. Crystallization and mechanical properties of the polylactide melt blown nonwovens. Fibers Polym. 2023;24:3101–14. https://doi.org/10.1007/s12221-023-00294-6.
29. Choi K, Choi M-C, Han D-H, Park T-S, Ha C-S. Plasticization of poly(lactic acid) (PLA) through chemical grafting of poly(ethylene glycol) (PEG) via in situ reactive blending. Eur Polymer J. 2013;49:2356–64. https://doi.org/10.1016/j.eurpolymj.2013.05.027.
30. Gardette M, Thérias S, Gardette J-L, Murariu M, Dubois P. Photooxidation of polylactide/calcium sulphate composites. Polym Degrad Stab. 2011;96:616–23. https://doi.org/10.1016/j.polymdegradstab.2010.12.023.
31. Zheng Y, Jia X, Zhao Z, Ran Y, Du M, Ji H, Pan Y, Li Z, Ma X, Liu Y, Duan L, Li X. Innovative natural antimicrobial natamycin incorporated titanium dioxide (nano-TiO_2)/ poly (butylene adipate-co-terephthalate) (PBAT) /poly (lactic acid) (PLA) biodegradable active film (NTP@PLA) and application in grape preservation. Food Chem. 2023;400:134100. https://doi.org/10.1016/j.foodchem.2022.134100.
32. Nepomuceno NC, Barbosa MA, Bonan RF, Oliveira JE, Sampaio FC, Medeiros ES. Antimicrobial activity of PLA/PEG nanofibers containing terpinen-4-ol against *Aggregatibacter actinomycetemcomitans*. J Appl Polym Sci. 2018;135:45782. https://doi.org/10.1002/app.45782.
33. Khakestani M, Jafari SH, Zahedi P, Bagheri R, Hajiaghaee R. Physical, morphological, and biological studies on PLA/NHA composite nanofibrous webs containing *e quisetum arvense* herbal extract for bone tissue engineering. J Appl Polym Sci. 2017;134:45343. https://doi.org/10.1002/app.45343.
34. Ahmadzadeh Y, Babaei A, Goudarzi A. Assessment of localization and degradation of ZnO nano-particles in the PLA/PCL biocompatible blend through a comprehensive rheological characterization. Polym Degrad Stab. 2018;158:136–47. https://doi.org/10.1016/j.polymdegradstab.2018.10.007.
35. Smith A, Wan C, Figiel Ł, Farris S, McNally T. Freestanding α-zirconium phosphate based nacre-like composite films cast from water. Compos Sci Technol. 2020;200:108443. https://doi.org/10.1016/j.compscitech.2020.108443.
36. Ran J, Xie H, Lai X, Li H, Zeng X. Significant improvement of tribological performances of polyamide 46/polyphenylene oxide alloy by functionalized zirconium phosphate. Tribol Int. 2018;128:204–13. https://doi.org/10.1016/j.triboint.2018.07.019.
37. Mazzanti V, Pariante R, Bonanno A, Ruiz de Ballesteros O, Mollica F, Filippone G. Reinforcing mechanisms of natural fibers in green composites: role of fibers morphology in a PLA/Hemp model system. Compos Sci Technol. 2019;180:51–9. https://doi.org/10.1016/j.compscitech.2019.05.015.
38. Maiza M, Benaniba MT, Quintard G, Massardier-Nageotte V. Biobased additive plasticizing polylactic acid (PLA). Polímeros. 2015;25:581–90. https://doi.org/10.1590/0104-1428.1986.
39. Liu Y, Ding Z, Liu X, Wang X, Zhang L. High thermodynamic stability study of PLA/LCNF composite. J Thermoplast Compos Mater. 2019;32:1017–30. https://doi.org/10.1177/0892705718779120.
40. González EA, Olmos D, Lorente MÁ, Vélaz I, González-Benito J. Preparation and characterization of polymer composite materials based on PLA/TiO_2 for antibacterial packaging. Polymers. 2018;10:1365. https://doi.org/10.3390/polym10121365.
41. Tarani E, Pušnik Črešnar K, Zemljič LF, Chrissafis K, Papageorgiou GZ, Lambropoulou D, Zamboulis A, Bikiaris ND, Terzopoulou Z. Cold crystallization kinetics and thermal degradation of PLA composites with metal oxide nanofillers. Appl Sci. 2021;11:300. https://doi.org/10.3390/app11073004.
42. Pandele AM, Constantinescu A, Radu IC, Miculescu F, Ioan Voicu S, Ciocan LT. Synthesis and characterization of PLA-micro-structured hydroxyapatite composite films. Materials. 2020;13:274. https://doi.org/10.3390/ma13020274.
43. Chu Z, Zhao T, Li L, Fan J, Qin Y. Characterization of antimicrobial poly (lactic acid)/nano-composite films with silver and zinc oxide nanoparticles. Materials. 2017;10:659. https://doi.org/10.3390/ma10060659.
44. Vasile C, Rapa M, Stefan M, Stan M, Macavei S, Darie-Nita RN, Barbu-Tudoran L, Vodnar DC, Popa EE, Stefan R, Borodi G, Brebu M. New Pla/ZnO:Cu/Ag bionanocomposites for food packaging. Express Polym Lett. 2017;11:531–44. https://doi.org/10.3144/expresspolymlett.2017.51.
45. Boopasiri S, Sae-Oui P, Roamcharern N, Jangpromma N, Ngernyen Y, Siriwong C. A bio-plastic composite film based on nanocrystalline cellulose-zinc oxide reinforced poly (lactic acid) with enhanced UV-shielding effect and antibacterial

activity for food packaging applications. Food Packag Shelf Life. 2023;38:101102. https://doi.org/10.1016/j.fpsl.2023.101102.